PHOTONICS Research

Ultracompact fiber laser based on a highly integrated optical device

Xiaoxiang Han and Xueming Liu*

State Key Laboratory of Modern Optical Instrumentation, Department of Optical Engineering, Zhejiang University, Hangzhou 310027, China
*Corresponding author: liuxm@zju.edu.cn

Received 24 July 2018; revised 28 October 2018; accepted 7 November 2018; posted 8 November 2018 (Doc. ID 340462); published 11 December 2018

The ultrafast fiber laser has attracted a great deal of research interest due to its low cost, high efficiency, and simple maintenance. Optical passive devices are vital parts of a fiber laser. In order to obtain a fiber laser with high quality, optical passive devices with high performance are required. Here, we demonstrate a highly integrated optical device with the combination of a saturable absorber (SA), coupler, isolator, wavelength division multiplexer, and erbium-doped fiber. The built-in SA has a modulation depth of 7% and can withstand high pump power due to the unique structure of the proposed device. The proposed device is applied to an ultracompact fiber laser, which greatly simplifies the laser structure and reduces the size of the proposed laser. The central wavelength, pulse duration, repetition rate, and signal-to-noise ratio of the output soliton are 1560 nm, 1.06 ps, 25.8 MHz, and 50 dB, respectively. The proposed device has great potential for application in high-power and high-frequency fiber lasers. The proposed ultracompact fiber laser has important applications in optical communication, optical sensing, optical frequency combs, and micromachining.

https://doi.org/10.1364/PRJ.7.000036

1. INTRODUCTION

The fiber laser is a highly important research field due to its inherent traits [1,2], such as high efficiency, high beam quality, simple maintenance, and compact structure. The fiber laser also has various applications [3–5] in optical communication, industry processing, optical information processing, micromachining, precision metrology, and medical imaging. Therefore, the fiber laser is expected to fully replace solid lasers as the new generation laser [6–8]. In order to meet the application demand, all-fiber lasers are required due to their low cost, high environmental stability, and easy integration [9–13]. Optical passive devices are vital components of a fiber laser. A fiber laser with excellent performance requires first-class optical passive devices [14]. Compared to a conventional optical device, an integrated optical device has multiple advantages of convenience, high compatibility, stable performance, and high reliability, which has attracted plenty of researchers' interest [15]. The integrated optical device has numerous applications, including optical communication, optical sensing technology, optical instruments, and so on [16]. It is highly important to improve the performance and integration level of optical passive devices.

In order to acquire an ultrafast pulse, two mode-locked techniques have been developed [17,18]. Actively mode-locked technology and passively mode-locked technology are the general classification methods [19]. Although actively mode-locked technology can generate high-repetition rate and narrow linewidth pulses, the active modulation device is not only expensive, but also jeopardizes the advantage of an all-fiber structure [20]. The passively mode-locked technique is a superior way to generate an ultrafast pulse [21]. The mode locker of the passively mode-locked technique is realized by nonlinear elements [22]. Different types of nonlinear elements, such as the nonlinear optical loop mirror (NOLM) [23], nonlinear polarization rotation (NPR) [24–26], semiconductor saturable absorption mirror (SESAM) [27], carbon nanotubes (CNTs) [28], graphene [29], and black phosphorus [30] are widely used as mode lockers. Among them, CNTs are ideal materials due to their low cost, high damage threshold, and subpicosecond recovery time. Generally, the CNT-based saturable absorber (SA) is independently sandwiched between two fiber connectors. The mode locker constructed by the above method has poor environmental stability and low damage threshold, which severely limits the application of CNT-based SAs. The evanescent field interaction with an SA by D-shape fiber or microfiber is another method to incorporate SA materials into a fiber laser [31,32]. The damage threshold of this method is increased by enlarging the interaction area between the laser beam and materials, but this method still has drawbacks, such as poor environmental stability and poor repeatability. At present, the hybrid optical device consists of couplers, isolators, and wavelength division multiplexers (WDMs), which are at a low level of integration [33]. Therefore, it is essential to integrate SAs

into the hybrid optical device, which can increase the damage threshold and environmental stability of the SA. The built-in SA also improves the integration level of optical devices.

In this paper, an ultracompact fiber laser based on a highly integrated optical device is proposed. The highly integrated optical device consists of an SA, optical coupler, isolator, WDM, and erbium-doped fiber (EDF), which greatly reduces the number of fiber laser components and simplifies the laser structure. The modulation depth of the built-in SA is estimated as 7%. The proposed device has important applications due to its compact structure and high damage threshold, so the advantages of an applied laser are high stability and miniaturization. The proposed all-fiber laser delivers ultrafast pulses with a central wavelength of ~1560 nm, pulse duration of 1.06 ps, repetition rate of 25.8 MHz, and signal-to-noise ratio (SNR) of 50 dB. The proposed optical device and fiber laser have great potential applications in the fields of optical communication, optical sensing, micromachining, and medical imaging.

2. EXPERIMENTAL SETUP

The proposed device consists of five functional components: an SA, coupler, isolator, WDM, and EDF. The internal schematic design of the proposed device is shown in Fig. 1(a). It can be seen that the functions of coupler and WDM are realized by a beam splitter and WDM slice, respectively. Those microdevices are attached to the end plane of a gradient-index lens (G-lens). The SA film is also placed on the end plane of the G-lens, which is after the beam splitter in this case. In the central section of the proposed device, the function of the isolator is realized by an isolator core, which is based on the Faraday effect. The isolator core consists of two wedges and a magneto-optical slice, which are enwrapped by a magnetic tube. The EDF is integrated into the dual-fiber pigtail. The light propagation path in the proposed device is as follows. The 1550 nm signal light is input from the EDF port of the front dual-fiber pigtail. The beam-splitting ratio of the coupler is 10/90, and 10% of the signal light is reflected back into the single-mode fiber (SMF) port of the front dual-fiber pigtail, which is used for fiber laser output. When the signal light passes through the SA film, the continuous wave (CW) becomes mode-locked due to its interaction with the SA film. The isolator core ensures unidirectional transmission of signal light. Then the signal light enters the dual-fiber collimator of the WDM and emits from the SMF port of the rear dual-fiber pigtail. The 980 nm pump light is input into the rear dual-fiber pigtail from the Hi-1060 fiber port, and reflected back to the SMF port, which will link to the EDF of the front dual-fiber pigtail and provide pump energy for the fiber laser. Figure 1(b) shows the image and size of the proposed optical device with a length of 24 mm and external diameter of 4 mm. The external diameter of the dual-fiber collimator is 2.7 mm, and the length of the outer glass tube is 18 mm. It can be seen that the proposed optical device is compact and miniaturized.

The SA film used in the proposed optical device is based on CNTs; its frame material is polyvinyl alcohol (PVA). The thickness of the SA film is about 30 μm. The absorption peak of the SA film is about 1600 nm, and the bandwidth is about 300 nm. The SA film is cut into a square shape with an area of about 1 mm^2. The details of SA preparation can be seen in Ref. [34]. The experiment setup of nonlinear optical absorption is illustrated in Fig. 2(a). A homemade ultrafast fiber laser centered at 1560 nm with the repetition rate of ~31.2 MHz and pulse duration of 1.18 ps is used as the laser source, and an attenuator is used to control the input power. The ultrafast pulse is split by a 10/90 optical coupler, and the output signals are monitored by two optical power meters simultaneously. The experimental data are fitted with a simplified two-level saturable absorption model $\alpha(I) = \alpha_{ns} + \frac{\alpha_0}{1+I/I_{sat}}$, where $\alpha(I)$ is the intensity-dependent absorption coefficient, α_0 is the linear limit of saturable absorption, α_{ns} is the nonsaturable absorption, and I_{sat} is the saturation intensity. The two-level saturable absorption model fits well with the experimental data, and the corresponding α_0, α_{ns}, and I_{sat} can be acquired. The modulation depth α_0 is estimated as 7%. The saturable intensity I_{sat} is about 5.25 MW/cm^2, and the nonsaturable absorption α_{ns} is approximately 32.5%.

The fabrication process of the proposed optical device includes the following steps. First, we integrate the gain fiber into

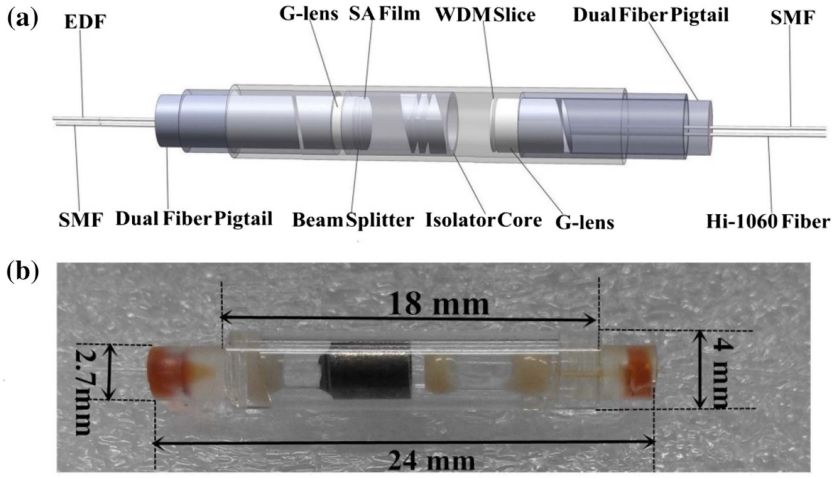

Fig. 1. (a) Internal schematic setup of the highly integrated optical device. EDF, erbium-doped fiber; SMF, single-mode fiber; G-lens, gradient-index lens; SA film, saturable absorber film; WDM slice, wavelength division multiplexer slice. (b) Image and size of the proposed optical device.

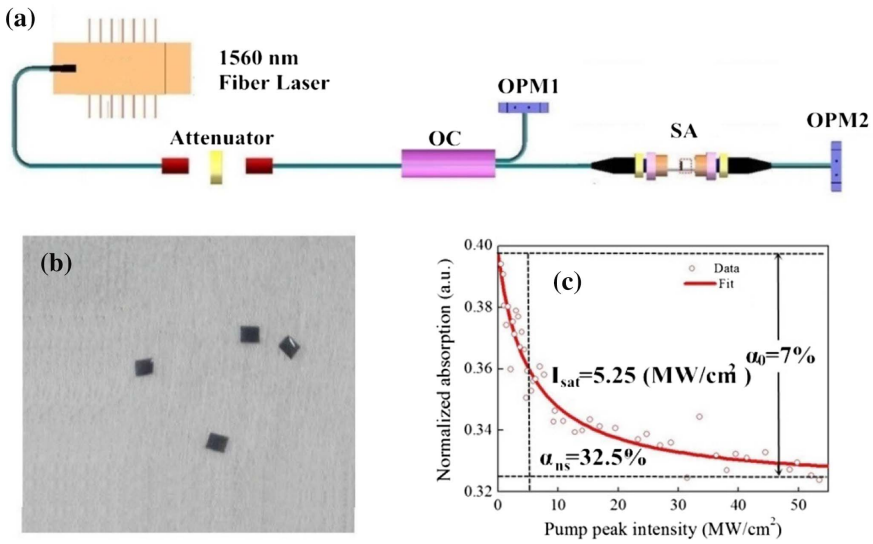

Fig. 2. (a) Schematic setup of nonlinear optical characterization. OC, optical coupler; OPM, optical power meter. (b) Image of SA film. (c) Nonlinear saturable absorption of the SA. The solid curve is the fit to the experimental data.

the front dual-fiber pigtail: the 10-mm long coating layer of gain fiber is stripped off with a clamp; then the gain fiber is dipped with 353ND glue, and inserted into one of the dual-fiber pigtail fine holes. The 353ND glue is heated and solidified with a curing oven. In order to acquire the dual-fiber pigtail with an 8° slope, the glass pigtail is ground with a lapping machine for multiple grinding cycles. We coat the glass pigtail with wide-spectrum antireflection film after the grinding process. Second, we assemble the dual fiber collimator of a coupler and WDM with a five-dimensional reflect-coupled system. The 8° slope of the dual-fiber pigtail and G-lens are carefully cleaned with a cotton swab and examined under a microscope for surface scratches or stains. We fix the G-lens first, and then observe the gap between them under a microscope, and adjusted the angle of the dual-fiber pigtail until their 8° slope is parallel. The G-lenses of coupler and WDM are adhered to with a 1550 nm 10/90 beam splitter and a 980/1550 nm WDM slice, respectively. The G-lens and dual-fiber pigtail are precisely adjusted with the five-dimensional reflect-coupled system until the insertion loss (IL) value is within a reasonable range. Here, the ILs of the coupler (splitting ratio of 10/90) and WDM are 10.5 and 0.5 dB, respectively. The G-lens and dual-fiber pigtail are pasted together by 3410-VM ultraviolet (UV) glue. The UV glue is irradiated with UV light for more than 20 s at a distance of 10–15 mm from the glue until the UV glue is completely solidified. Third, the SA film and isolator core are integrated on the dual-fiber collimator plane of the coupler. The paste process is described as follows. We carefully clean the G-lens surface with a cotton swab dipped in alcohol. Then a small amount of UV glue is placed on four edges of the SA film. We place the SA film on the G-lens surface and irradiate it with UV light. The isolator core is placed onto the G-lens head after the SA, and the junction is coated with UV glue and illuminated with UV light. Fourth, the ready-made coupler with isolator core and WDM is precisely adjusted by a five-dimensional transmit-coupled system. The alignment of the spatial optical path is accurately controlled until the IL meets the requirements. Here, the transmitted IL of the proposed device is 6.5 dB due to the 10/90 splitting ratio of the coupler, SA film, 3.3-m EDF, and single-stage isolator core. Then a glass tube is used to encapsulate the already adjusted components. By injecting UV glue onto the junction, the relative positions of each component are permanently fixed.

The proposed device is applied in an ultracompact mode-locked fiber laser. The schematic setup of the proposed fiber laser is shown in Fig. 3. The separate passive devices, namely, the WDM, coupler, isolator, SA, and EDF, are integrated into the proposed device, so the fiber laser is greatly simplified due to the proposed device. Since fiber has the advantages of high flexibility and small diameter, the size of the proposed fiber laser can be greatly reduced. The isolator core in the proposed device is used to realize unidirectional transmission, the 10/90 coupler port is utilized to extract the pulses from the laser cavity, the 980 nm pump energy of a laser diode (LD) is input into the laser cavity from the WDM port, and the SA film works as a mode-locker. The EDF in the proposed device is 3.3-m long and pumped by the LD with the maximum output power of 550 mW. The cavity dispersion can be controlled by altering the length of the SMF. The red arrow in the inner loop shows the propagation route of 980 nm light, while the blue arrow in the outer loop shows the propagation route of the 1550 nm CW and soliton. An optical spectrum analyzer, an autocorrelator (AC), a radio-frequency (RF) analyzer with a photodiode detector, and a 6-GHz digital oscilloscope are used to monitor the pulse spectrum, duration, repetition rate, and sequence simultaneously.

3. EXPERIMENTAL RESULTS AND ANALYSES

The ultrafast pulse is achieved in the following fiber laser setup, which includes a 3.3-m EDF with a group velocity dispersion (GVD) of $-16\ \mathrm{ps\cdot nm^{-1}\cdot km^{-1}}$ and a 4.6-m SMF with a GVD

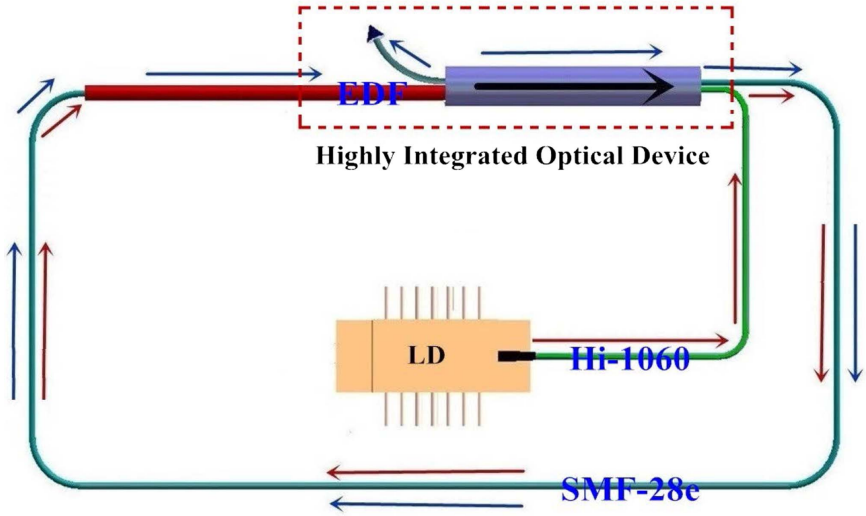

Fig. 3. Schematic setup of the ultracompact laser. EDF, erbium-doped fiber; the highly integrated optical device is marked with a red dashed rectangle box, and it is an aggregation of an SA, coupler, isolator, WDM, and EDF; LD, laser diode. The red arrow in the inner loop shows the propagation route of 980-nm light, while the blue arrow in the outer loop shows the propagation route of the 1550-nm CW and soliton.

of 17 ps · nm^{-1} · km^{-1}. The net cavity dispersion β^2 is calculated as about −0.03 ps^2. At the pump power of ∼18 mW, a CW is established. When the total pump power is increased to ∼30 mW, mode-locking can be self-started. Figure 4(a) shows the laser spectrum with a central wavelength of ∼1560 nm and 3-dB bandwidth of 4 nm. Figure 4(b) illustrates the corresponding oscilloscope trace. The pulse-to-pulse separation is 38.7 ns, which is equal to the cavity length of 7.9 m. The full width at half-maximum (FWHM) of the autocorrelation trace in Fig. 4(c) is 1.63 ps. The pulse duration is estimated as 1.06 ps with a sech^2 fit shown by a blue solid line. Since the net cavity dispersion approaches zero (i.e., −0.03 ps^2), a soliton propagating in such a cavity is stretched and compressed periodically. Thanks to the periodic stretching and compression of the soliton, nonlinear effects are decreased, and the pulse can accumulate large energy with a broad spectrum and large pulse duration. Consequently, the time bandwidth product (TBP) of the proposed soliton is calculated as 0.529, meaning that the pulses are slightly chirped, and its pulse duration can be compressed to 0.63 ps, theoretically. Figure 4(d) shows that the repetition rate of the fundamental cavity frequency is 25.834 MHz, corresponding to 38.7 ns of round-trip time in Fig. 4(b). The RF spectrum gives an SNR of 50 dB, indicating low-amplitude fluctuations and good

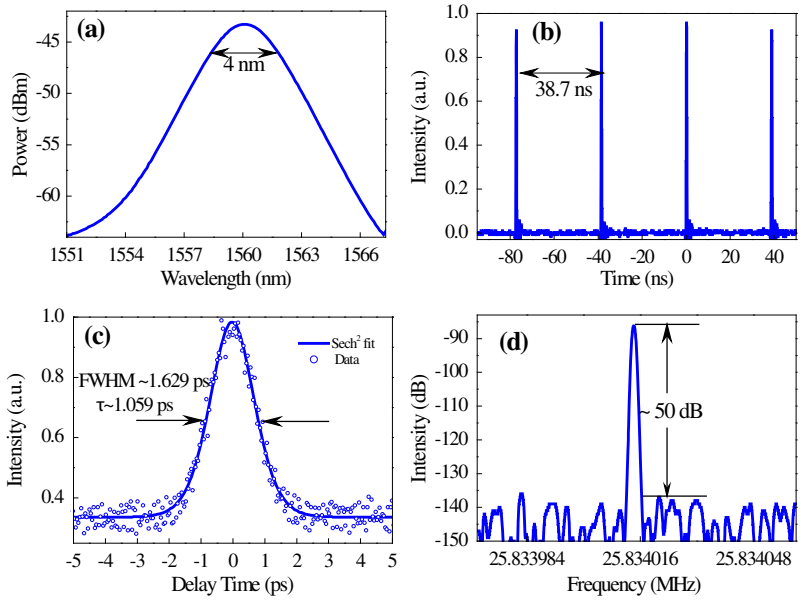

Fig. 4. Typical characteristics of an ultrafast soliton. (a) Optical spectrum; (b) oscilloscope trace; (c) autocorrelation trace of the experimental data (circles) and sech^2-shaped fit (solid curve); (d) fundamental RF spectrum.

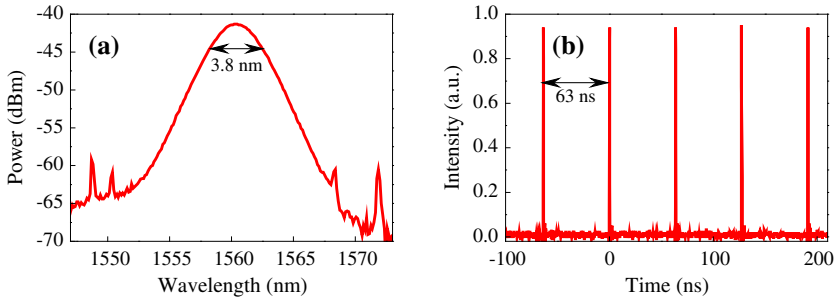

Fig. 5. Characteristics of ultrafast CS. (a) Optical spectrum; (b) oscilloscope trace.

mode-locking stability of the obtained soliton. The average power of the output pulse is about 300 μW.

Depending on the setting of cavity dispersion, different mode-locked pulses can be achieved in the proposed fiber laser, and a dispersion management design can be proposed [34]. When we add a section of SMF (~5 m) to the laser resonant cavity, the net cavity dispersion β^2 is calculated as about −0.14 ps^2, and thus conventional soliton (CS) tends to be formed in the fiber laser. At the pump power of ~25 mW, mode-locking of CS can be self-started. Figure 5(a) shows the typical laser spectrum of a CS with sidebands. The sidebands stem from the constructive interference between the soliton and dispersive waves, when the soliton suffers from periodic perturbations [34]. Figure 5(b) illustrates the corresponding oscilloscope trace of a CS. The pulse-to-pulse separation is 63 ns, which is equal to the cavity length of 12.9 m. The experimental results illustrate that the proposed device can be utilized in a fiber laser to generate an ultrafast pulse. The average power of a CS is about 120 μW.

The SA film is usually sandwiched between two fiber ferrules inside a physical contact ferrule connector. However, the damage threshold of this method is low due to the small waist radius of the laser beam in the fiber core. The laser beam in the proposed device passes through the G-lens before it interacts with the SA film, so the waist radius of the laser beam is amplified. According to the principle of the G-lens, the beam radius is calculated as [35] $\omega_1 = \frac{\lambda}{n_0\sqrt{A}\pi\omega_0}$, where ω_0 and ω_1 stand for the beam radius before and after the beam passes through the G-lens, respectively; λ is the operating wavelength, n_0 is the axis refractive index of the G-lens, and $\sqrt{A}$ is the focusing constant of the G-lens. We use the following parameters for matching the experimental conditions: $\omega_0 = 5$ μm, $\lambda = 1550$ nm, $n_0 = 1.5975$, $\sqrt{A} = 0.5795$ mm^{-1}, and $\omega_1 = 100$ μm, which is about 20 times larger than the beam radius in an SMF. So, the damage threshold of the proposed device is hundreds of times larger than that of an SA sandwiched between fiber ferrules, in theory. The method of evanescent field interaction with the SA has poor environmental stability. Since the evanescent field is released from the fiber, the optical field became sensitive to the external disturbance without the protection of fiber. The SA in the proposed device is encapsulated in a sealed glass tube, which is immune to external disturbance. The proposed device has the advantages of high energy resistance and high environmental stability. In our experiment, solitons can always be observed when the pump power is raised from the self-starting threshold to the maximum available power (550 mW). When the pump power increases to 550 mW, the SNR of the output pulse is about 50 dB. The built-in SA has excellent long-term stability. For a fiber laser, the mode-locked operation can be maintained for weeks. The chemical stability of CNT-SA is also important. The ready-made SA remains intact for years, and a mode-locking operation can also be achieved.

4. CONCLUSIONS

In this paper, we have demonstrated a highly integrated optical device with a modulation depth of 7% and an ultracompact fiber laser. The proposed device reduces the number of fiber laser components to two, namely, an LD and the proposed device. As a result, the size and design of the fiber laser can be greatly decreased and simplified, respectively. The normal gain fiber of the optical device can also be replaced with heavily doped gain fiber, which paves the way for a high-repetition-rate fiber laser. Moreover, there is residual space to incorporate another micro-optical device (i.e., spectral filter device, high gain medium) into the proposed device, and further increase the integration degree of the proposed device. The ultracompact fiber laser delivers a stable ultrafast pulse with a central wavelength of ~1560 nm, pulse duration of 1.06 ps, repetition rate of 25.8 MHz, and SNR of 50 dB, which can be employed as a source of the laser amplification system. The proposed optical device and fiber laser have numerous applications in optical communication, optical sensing, optical frequency combs, micromachining, and medical imaging.

Funding. National Natural Science Foundation of China (NSFC) (61525505, 11774310, 61805212); China Postdoctoral Science Foundation (2017M621918); Key Scientific and Technological Innovation Team Project in Shaanxi Province (2015KCT-06).

REFERENCES

1. G. Krauss, S. Lohss, T. Hanke, A. Sell, S. Eggert, R. Huber, and A. Leitenstorfer, "Synthesis of a single cycle of light with compact erbium-doped fibre technology," Nat. Photonics **4**, 33–36 (2010).
2. M. E. Fermann and I. Hartl, "Ultrafast fiber laser technology," IEEE J. Sel. Top. Quantum Electron. **15**, 191–206 (2009).
3. G. P. Agrawal, *Applications of Nonlinear Fiber Optics* (Academic, 2010).

4. X. Liu, X. Yao, and Y. Cui, "Real-time observation of the buildup of soliton molecules," Phys. Rev. Lett. **121**, 023905 (2018).
5. F. Chen and J. V. de Aldana, "Optical waveguides in crystalline dielectric materials produced by femtosecond laser micromachining," Laser Photon. Rev. **8**, 251–275 (2014).
6. T. Eidam, S. Hanf, E. Seise, T. Andersen, T. Gabler, C. Wirth, T. Schreiber, J. Limpert, and A. Tünnermann, "Femtosecond fiber CPA system emitting 830 W average output power," Opt. Lett. **35**, 94–96 (2010).
7. B. Oktem, C. Ulgudur, and F. Ilday, "Soliton-similariton fibre laser," Nat. Photonics **4**, 307–311 (2010).
8. X. Liu and Y. Cui, "Flexible pulse-controlled fiber laser," Sci. Rep. **5**, 9399 (2015).
9. Z. Qiao, L. C. Kong, G. Q. Xie, Z. P. Qin, P. Yuan, L. J. Qian, X. D. Xu, J. Xu, and D. Y. Fan, "Ultraclean femtosecond vortices from a tunable high-order transverse-mode femtosecond laser," Opt. Lett. **42**, 2547–2550 (2017).
10. F. W. Wise, A. Chong, and W. H. Renninger, "High-energy femtosecond fiber lasers based on pulse propagation at normal dispersion," Laser Photon. Rev. **2**, 58–73 (2008).
11. X. Liu, "Mechanism of high-energy pulse generation without wave breaking in mode-locked fiber lasers," Phys. Rev. A **82**, 053808 (2010).
12. N. Nyushkov, V. Ivanenko, S. M. Kobtsev, K. Turitsyn, C. Mou, L. Zhang, V. I. Denisov, and V. S. Pivtsov, "Gamma-shaped long-cavity normal-dispersion mode-locked Er-fiber laser for sub-nanosecond high-energy pulsed generation," Laser Phys. Lett. **9**, 59–67 (2012).
13. Y. Cui, F. Lu, and X. Liu, "Nonlinear saturable and polarization-induced absorption of rhenium disulfide," Sci. Rep. **7**, 40080 (2017).
14. N. Ansari and Y. Luo, *Passive Optical Device: Computer Science and Communications Dictionary* (Springer, 2011), p. 1235.
15. P. Sah and B. K. Das, "Integrated optical rectangular-edge filter devices in SOI," IEEE J. Lightwave Technol. **35**, 128–135 (2017).
16. S. Li and D. Gao, "Integrated optical device design based on transformation optics," in *Progress in Electromagnetic Research Symposium* (2016), p. 16.
17. Y. Zhou, A. Wang, C. Gu, B. Sun, L. Xu, F. Li, D. Chung, and Q. Zhan, "Actively mode-locked all fiber laser with cylindrical vector beam output," Opt. Lett. **41**, 548–550 (2016).
18. J. B. Schröder, S. Coen, T. Sylvestre, and B. J. Eggleton, "Dark and bright pulse passive mode-locked laser with in-cavity pulse-shaper," Opt. Express **18**, 22715–22721 (2010).
19. S. Kobtsev, S. Kukarin, S. Smirnov, S. Turitsyn, and A. Latkin, "Generation of double-scale femto/pico-second optical lumps in mode-locked fiber lasers," Opt. Express **17**, 20707–20713 (2009).
20. H. Q. Lam, P. Shum, Y. D. Gong, and S. Fu, "Series analysis of active mode-locked laser under the influence of ASE noise," J. Lightwave Technol. **26**, 1671–1680 (2008).
21. X. Liu, "Hysteresis phenomena and multipulse formation of a dissipative system in a passively mode-locked fiber laser," Phys. Rev. A **81**, 023811 (2010).
22. X. Liu, Y. Cui, D. Han, X. Yao, and Z. Sun, "Distributed ultrafast fibre laser," Sci. Rep. **5**, 9101 (2015).
23. L. M. Zhao, A. C. Bartnik, Q. Q. Tai, and F. W. Wise, "Generation of 8 nJ pulses from a dissipative-soliton fiber laser with a nonlinear optical loop mirror," Opt. Lett. **38**, 1942–1944 (2013).
24. X. Wang, P. Zhou, X. Wang, H. Xiao, and Z. Liu, "Pulse bundles and passive harmonic mode-locked pulses in Tm-doped fiber laser based on nonlinear polarization rotation," Opt. Express **22**, 6147–6153 (2014).
25. L. J. Kong, L. M. Zhao, S. Lefrancois, D. G. Ouzounov, C. X. Yang, and F. W. Wise, "Generation of megawatt peak power picoseconds pulses from a divided-pulse fiber amplifier," Opt. Lett. **37**, 253–255 (2012).
26. W. Wang, H. Meng, X. Wu, W. Wang, R. Xiong, H. Xue, C. Tan, and X. Huang, "A nonlinear polarization rotation-based linear cavity waveband switchable multi-wavelength fiber laser," Laser Phys. Lett. **10**, 015104 (2013).
27. C. Ouyang, P. Shum, K. Wu, J. Wong, H. Lam, and S. Aditya, "Bidirectional passively mode-locked soliton fiber laser with a four-port circulator," Opt. Lett. **36**, 2089–2091 (2011).
28. Y. W. Song, S. Yamashita, and S. Maruyama, "Single-walled carbon nanotubes for high-energy optical pulse formation," Appl. Phys. Lett. **92**, 021115 (2008).
29. F. Bonaccorso, Z. Sun, T. Hasan, and A. Ferrari, "Graphene photonics and optoelectronics," Nat. Photonics **4**, 611–622 (2010).
30. Z. P. Qin, G. Q. Xie, C. J. Zhao, S. C. Wen, P. Yuan, and L. J. Qian, "Mid-infrared mode-locking pulse generation with multilayer black phosphorus as saturable absorber," Opt. Lett. **41**, 56–59 (2016).
31. J. H. Im, S. Choi, F. Rotermund, and D. Yeom, "All-fiber Er-doped dissipative soliton laser based on evanescent field interaction with carbon nanotube saturable absorber," Opt. Express **18**, 22141–22146 (2010).
32. P. Yan, R. Lin, S. Ruan, A. Liu, and H. Chen, "A 2.95 GHz, femtosecond passive harmonic mode-locked fiber laser based on evanescent field interaction with topological insulator film," Opt. Express **23**, 154–164 (2015).
33. M. Schumann, T. Bückmann, N. Gruhler, M. Wegener, and W. Pernice, "Hybrid 2D-3D optical devices for integrated optics by direct laser writing," Light Sci. Appl. **3**, e175 (2014).
34. X. Liu, D. Han, Z. Sun, C. Zeng, H. Lu, D. Mao, Y. Cui, and F. Wang, "Versatile multi-wavelength ultrafast fiber laser mode-locked by carbon nanotubes," Sci. Rep. **3**, 2718 (2013).
35. Y. Fan, X. Roux, A. Korovin, A. Lupu, and A. Lustrac, "Integrated 2D-graded index plasmonic lens on a silicon waveguide for operation in the near infrared domain," ACS Nano **11**, 4599–4605 (2017).